Chinese Journal of
POLYMER SCIENCE

RESEARCH ARTICLE

https://doi.org/10.1007/s10118-022-2719-z
Chinese J. Polym. Sci. **2022**, *40*, 889–897

Subtle Effect of Alkyl Substituted *π*-Bridges on Dibenzo[*a*,*c*]phenazine Based Polymer Donors towards Enhanced Photovoltaic Performance

Chun-Xian Ke[a,†], Xue Lai[a,†], Heng-Tao Wang[a], Ming-Rui Pu[a], Tahir Rehman[a], Yu-Lin Zhu[a], and Feng He[a,b*]

[a] *Shenzhen Grubbs Institute and Department of Chemistry, Southern University of Science and Technology, Shenzhen 518055, China*
[b] *Guangdong Provincial Key Laboratory of Catalysis, Southern University of Science and Technology, Shenzhen 518055, China*

Electronic Supplementary Information

Abstract Selection of the strategically substituted alkyl chains has a significant effect to modulate the physical properties of conjugated polymers, electro-optical characteristics, and active layer morphology of the corresponding polymer solar cells (PSCs). Herein, we systematically synthesized three dibenzo[*a*,*c*]phenazine based D-*π*-A donor polymers named PBP-C0, PBP-C8, and PBP-C6 with different alkyl substitutions on thiophene *π*-bridges, without alkyl, 2-ethylhexyl and *n*-hexyl groups, respectively. The absence of the alkyl chain (PBP-C0) on the *π*-bridge caused poor solubility and unfavorable miscibility with the Y5 acceptor, leading to the lower photovoltaic performance. The bulky alkyl chain of 2-ethylhexyl on the *π*-bridge group caused the twisting of PBP-C8 conjugated backbone, which limits the charge transport and also compromises the photovoltaic performance. In contrast, the PBP-C6-with flexible linear alkyl chains has almost planar curvature geometry resulting in the small uniform domain size and appropriate phase separation in the blend film morphology. These favorable properties enhanced the exciton generation to dissociation, charge carrier mobility, and also lowered the charge recombination. Among three polymers, PBP-C6-based devices exhibit the best PCE of 11.60%. From these results, thiophene *π*-bridge alkyl substitution demonstrated an important strategy to adjust energy level, absorption, and phase separation morphology to enhance the photovoltaic performance of the PSCs.

Keywords *π*-Bridge; Alkyl chain engineering; Phenazine; Polymer donor; Polymer solar cell

Citation: Ke, C. X.; Lai, X.; Wang, H. T.; Pu, M. R.; Rehman, T.; Zhu, Y. L.; He, F. Subtle effect of alkyl substituted *π*-bridges on dibenzo[*a*,*c*]phenazine based polymer donors towards enhanced photovoltaic performance. *Chinese J. Polym. Sci.* **2022**, *40*, 889–897.

INTRODUCTION

Polymer solar cells (PSCs) have gained a lot of attention from researchers attributed to inherent advantages, flexibility, lightweight, low cost, easy solution processability, and potential commercial large-scale layer to layer production.[1–10] Recently, the power conversion efficiency (PCE) of PSCs has been enhanced dramatically after the emergence of the Y-series of non-fullerene acceptors with a unique A-D-A`-D-A structure. In 2019, Y6 non-fullerene acceptor was discovered by Zou and co-workers, exhibiting an impressive PCE of 15.7% with the star donor polymer PM6.[11,12] Since then many research groups performed rational structural derivatization to further boost photovoltaic performance.[13–16] As Y-series acceptors demonstrated extraordinary performances, it is highly requisite to design the highly efficient complementary polymer donors. Therefore, researchers put forward many efforts to design novel efficient polymer donors and also to improve the already known molecular structure. PM6 is the most frequently used star high-performance D-*π*-A donor polymer, reported by Hou and co-workers in 2015, where 4,8-bis(5-(2-ethylhexyl)-4-fluorothiophen-2-yl)benzo[1,2-*b*:4,5-*b*′] (BDT-F) was employed as electron-rich (D) unit and 1,3-bis(thiophen-2-yl)-5,7-bis(2-ethylhexyl)benzo-[1,2-*c*:4,5-*c*′]dithiophene-4,8-dione (BDD) as electron deficient (A) unit.[11] PM6 remains the first choice to realize the high-performance PSC, it is evident that most of the efficient PSCs over 17% are fabricated with PM6 as a donor.[17–23] Meanwhile, there are several other noticeable high-performance donor polymers based on binary devices reported, PBTT-F,[24] D18,[25] PBD-Cl,[26] BNTB-2T[27] and PBQ6.[28]

In 2018, Li and co-workers reported a quinoxaline-based polymer donor PTQ10, where difluorinated-alkoxy-substituted quinoxaline (DFQ) was employed as (A) unit and thiophene as (D) unit, realized the PCE of 12.7% with IDIC as acceptor.[29] To further reveal the potential of quinoxaline, they developed high-performance polymers.[24] The availability of multiple substitution sites on quinoxaline units provides an exceptional advantage to modulate electro-optical properties along with the film morphology. Compared to pendant phenyl ring on quinoxaline, cyclized dibenzo[*a*,*c*]phenazine has more planarity and extended conjugation. In previous reports, dibenzo[*a*,*c*]phenazine unit copolymerized with several other

* Corresponding author, E-mail: hef@sustech.edu.cn
† These authors contributed equally to this work.
Special Issue: Organic Photovoltaic Polymers
Received January 4, 2022; Accepted February 17, 2022; Published online May 20, 2022

electron-rich units, carbazole,[30] fluorene,[31] IDT,[32,33] and BDT,[34–37] but the binary devices based on those materials only delivered PCEs around 5%, according to the best of our knowledge.

Herein, we employed quinoxaline derivative dibenzo[*a*,*c*] phenazine as (A) unit to construct D-*π*-A polymers with BDT-F as (D) unit. We rationally used different alkyl-substituted thiophene *π*-bridge to synthesize polymer named as PBP-C0, PBP-C8, and PBP-C6 with non-alkylated, 2-ethylhexyl, and *n*-hexyl alkyl chains on thiophene bridge, respectively. To design new D-*π*-A based polymers, *π*-bridges play a critical role to regulate the conjugated backbone conformation and molecular geometry.[38–44] Therefore, the introduction of *π*-bridges requires careful consideration due to the subtle effects on the electro-optical properties, structure geometry, film morphology, processability, and photovoltaic performance. In general, weak electron-donating thiophene derivatives as *π*-bridges have a reputation to achieve balance in intrinsic properties and processability.[45–48] Both PBP-C0 and PBP-C8 exhibited low photovoltaic performance because of the poor solubility and twisted conjugated backbone, respectively. Whereas in a previous report, the introduction of alkyl-substituted *π*-bridge induces twisted zigzag conformation allowing easy solution processability to realize the high performance for BDD-based polymers.[49] PBP-C6 with *n*-hexyl substituted thiophene *π*-bridge relatively have a planar conjugated backbone. The binary devices based on PBP-C6:Y5 demonstrated the best PCE of 11.6%. To the best of our knowledge, we are reporting the highest PCE of dibenzo[*a*,*c*] phenazine-based binary devices as 11.6% with Y5 as acceptor. These results reveal the subtle effect of alkyl groups on *π*-bridge to control the optical properties, energy levels, solubility, and phase separation morphology, which all are essential to developing efficient polymer donors.

EXPERIMENTAL

Materials and Measurements

The synthetic routes to the three target polymers, PBP-C0, PBP-C8 and PBP-C6, are fully illustrated in Scheme 1. All chemicals in this study were purchased from commercial resources unless additional noted. Compounds **2**, **3**, and **4** were synthesized according to the previous report.[50] ^{1}H-NMR was used to characterize all the molecules. Besides, ^{13}C-NMR and matrix-assisted laser desorption ionization time-of-flight mass spectrometry (MALDI-TOF MS) were used to characterize the three monomers.

Synthesis of Compound 6

The solution of compound **5** (3.0 g, 10.28 mmol) in anhydrous ethanol was prepared. Then, 12 g (290 mmol) of $NaBH_4$ was added in small batches at 0 °C. After 10 min reaction, the mixture was gradually raised to room temperature and stirred overnight. After the evaporation of ethanol, the solid was dissolved in dichloromethane and washed with saturated brine

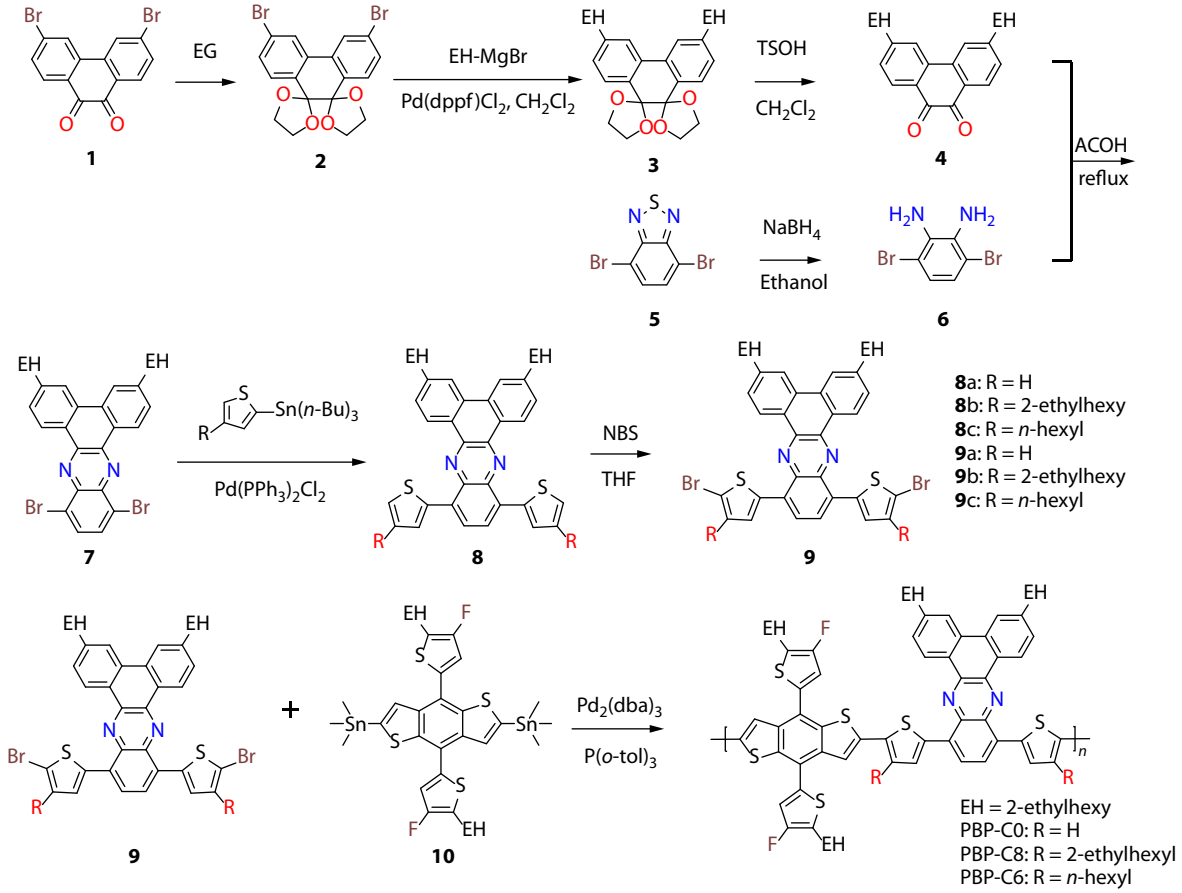

Scheme 1 Synthetic routes to PBP-C0, PBP-C8 and PBP-C6 polymers.

https://doi.org/10.1007/s10118-022-2719-z

for three times. The organic phase was dried with sodium sulfate and the solvent was evaporated after filtration to obtain white solid compound **6**. The crude product can be used in the next reaction without further purification.

Synthesis of Compound 7

Under an argon atmosphere, compound **4** (1.0 g, 2.31 mmol) and compound **6** (0.74 g, 2.78 mmol) were dissolved in acetic acid (50 mL) and refluxed overnight. Then, the temperature of the reaction mixture was brought to room temperature, the yellow solid appeared in the liquor. The yellow solid compound **7** (0.78 g, yield=42%) was obtained from silica column chromatography by using hexane as the eluent. ^{1}H-NMR (400 MHz, Chloroform-d, δ, ppm) 9.31 (d, J=8.1 Hz, 2H), 8.25 (s, 2H), 7.96 (s, 2H), 7.55 (d, J=8.6 Hz, 2H), 2.84 (d, J=7.1 Hz, 4H), 1.84–1.75 (m, 2H), 1.42–1.29 (m, 16H), 0.9–0.90 (m, 12H).

Synthesis of Compound 8a

The Stille-coupling reaction was carried out to acquire compound **8**a. Compound **7** (0.25 g, 0.39 mmol) and tributyl(thiophen-2-yl)stannane (0.59 g, 1.58 mmol) were added in a sealed flask with $Pd(PPh_3)_2Cl_2$ (20 mg, 0.019 mmol) as catalyst. Vacuuming and backfilling the flask with argon gas three times to ensure oxygen free system. After adding 20 mL of deoxygenated toluene as solvent, the temperature of the reaction mixture was raised to 110 °C and kept stirring overnight. After completion of the reaction, the toluene was removed through a rotary evaporator and further subjected to silica column chromatography to give a red solid product **8**a (0.90 g, yield=71%), hexane:dichloromethane (9:1) as the eluent. ^{1}H-NMR (400 MHz, Chloroform-d, δ, ppm) 9.47 (d, J=8.1 Hz, 2H), 8.32 (s, 2H), 8.23 (s, 2H), 7.92 (d, J=3.2 Hz, 2H), 7.65 (d, J=5.2 Hz, 2H), 7.62 (d, J=8.2 Hz, 2H), 7.28 (s, 2H), 2.86 (d, J=7.1 Hz, 4H), 1.85–1.76 (m, 2H), 1.37–1.31 (m, 24H), 0.97–0.88 (m, 12H).

Synthesis of Compound 8b

Compound **8**b (0.26 g, 0.29 mmol, yield=88%) was obtained by using the same reaction conditions as the synthesis of compound **8**a with compound **7** (0.22 g, 0.33 mmol) and tributyl(4-(2-ethylhexyl)thiophen-2-yl)stannane (0.65 g, 1.33 mmol). ^{1}H-NMR (400 MHz, Chloroform-d, δ, ppm) 9.47 (d, J=8.2 Hz, 2H), 8.31 (s, 2H), 8.18 (s, 2H), 7.76 (s, 2H), 7.60 (d, J=8.2 Hz, 2H), 7.20 (s, 2H), 2.86 (d, J=7.1 Hz, 4H), 2.73–2.66 (m, 4H), 1.84–1.70 (m, 5H), 1.45–1.32 (m, 33H), 0.95–0.89 (m, 24H).

Synthesis of Compound 8c

Compound **8**c (0.34 g, 0.41 mmol, yield=84%) was obtained by using the same reaction conditions as the synthesis of compound 8a with compound 7 (0.32 g, 0.48 mmol) and tributyl(4-hexylthiophen-2-yl)stannane (0.90 g, 1.96 mmol). ^{1}H-NMR (400 MHz, Chloroform-d, δ, ppm) 9.45 (d, J=8.2 Hz, 2H), 8.30 (s, 2H), 8.16 (s, 2H), 7.77 (d, J=1.5 Hz, 2H), 7.59 (d, J=8.2 Hz, 2H), 7.22 (s, 2H), 2.85 (d, J=7.1 Hz, 4H), 2.75 (t, J=7.7 Hz, 4H), 1.83–1.74 (m, 6H), 1.40–1.37 (m, 32H), 0.98–0.87 (m, 18H).

Synthesis of Monomer 9a

Under the dark condition *N*-bromosuccinimide (NBS) (0.143 g, 0.81mmol) was added to solution of compound **8**a (0.27 g, 0.40 mmol) in 30 mL of THF at 0 °C. After the removal of ice bath, the reaction mixture was kept on stirring for 2 h at room temperature. The reaction was quenched by the addition of 10 ml water. A red solid product compound **9**a (0.21 g, yield=63%) was obtained from silica column chromatography with hexane as the eluent. ^{1}H-NMR (400 MHz, Chloroform-d, δ, ppm) 9.23 (d, J=8.0 Hz, 2H), 8.21 (s, 2H), 7.94 (s, 2H), 7.57 (d, J=8.0 Hz, 2H), 7.47 (d, J=3.2 Hz, 2H), 7.12 (d, J=3.0 Hz, 2H), 2.83 (d, J=6.4 Hz, 4H), 1.82 (s, 2H), 1.44–1.31 (m, 16H), 1.00–0.89 (m, 12H). ^{13}C-NMR (101 MHz, Chloroform-d, δ, ppm) 144.61, 141.79, 139.50, 137.07, 132.14, 130.10, 129.21, 128.92, 127.93, 127.75, 125.17, 124.91, 123.05, 116.71, 41.20, 40.90, 32.51, 28.96, 25.63, 23.18, 14.26, 10.93. MALDI-TOF MS: calculated for $C_{44}H_{46}Br_2N_2S_2$ [M^+]: 826.7940; Found: 826.1855.

Synthesis of Monomer 9b

Monomer **9**b (2.0 g, 1.90 mmol, yield=85%) was obtained by using the same condition as the synthesis of compound **9**a, with compound **8**b (2.0 g, 2.24 mmol) and NBS (0.83 g, 4.70 mmol). ^{1}H-NMR (400 MHz, Chloroform-d, δ, ppm) 9.34 (d, J=8.1 Hz, 2H), 8.24 (s, 2H), 8.04 (s, 2H), 7.59 (d, J=8.3 Hz, 2H), 7.50 (s, 2H), 2.84 (d, J=7.0 Hz, 4H), 2.61 (d, J=7.1 Hz, 4H), 1.85–1.72 (m, 4H), 1.46–1.30 (m, 32H), 1.00–0.87 (m, 24H). ^{13}C-NMR (101 MHz, Chloroform-d, δ, ppm) 144.29, 141.52, 140.02, 137.46, 137.32, 131.97, 129.94, 129.04, 127.96, 127.71, 126.36, 124.61, 122.89, 114.55, 41.17, 40.91, 40.16, 33.84, 32.64, 32.53, 28.95, 25.75, 25.63, 23.24, 23.21, 14.28, 10.97, 10.93. MALDI-TOF MS: calculated for $C_{60}H_{78}Br_2N_2S_2$ [M^+]: 1051.2260; Found: 1051.5098.

Synthesis of Monomer 9c

Monomer **9**c (0.74 g, 0.75 mmol, yield=70%) was obtained by using the same condition as the synthesis of compound **9**a, with compound **8**c (0.90g, 1.08 mmol) and NBS (0.40 g, 2.26 mmol). ^{1}H-NMR (400 MHz, Chloroform-d, δ, ppm) 9.37 (d, J=8.2 Hz, 2H), 8.28 (s, 2H), 8.06 (s, 2H), 7.62 (d, J=8.2 Hz, 2H), 7.55 (s, 2H), 2.85 (d, J=7.1 Hz, 4H), 2.69 (t, J=7.7 Hz, 4H), 1.82 (t, J=6.2 Hz, 2H), 1.73 (s, 4H), 1.50–1.28 (m, 28H), 0.99–0.92 (m, 18H). ^{13}C-NMR (101 MHz, Chloroform-d, δ, ppm) 144.13, 141.33, 140.70, 137.47, 137.06, 131.87, 129.66, 128.91, 127.94, 127.70, 125.56, 124.29, 122.80, 113.72, 41.16, 40.89, 32.53, 31.87, 29.92, 29.65, 29.31, 28.98, 25.62, 23.22, 22.81, 14.29, 14.25, 10.92. MALDI-TOF MS: calculated for $C_{56}H_{70}Br_2N_2S_2$ [M^+]: 995.1180; Found: 995.4521.

Polymerization of PBP-C0, PBP-C8, and PBP-C6

Polymers PBP-C0, PBP-C8, and PBP-C6 were synthesized through the Stille-coupling reaction of **10** with **9**a, **9**b, and **9**c, respectively, where $Pd_2(dba)_3$ was used as a catalyst and P(*o*-tol)$_3$ as ligand, in deoxygenated toluene, under an argon atmosphere. The reaction mixture was kept on stirring overnight at 125 °C in an oil bath. The reaction mixture was dropped in methanol and the precipitates were collected through vacuum filtration. Polymers were extracted from Soxhlet extraction using methanol, petroleum ether, dichloromethane, chloroform, and chlorobenzene, successively. PBP-C8 and PBP-C6 exhibited good solubility in chloroform and chlorobenzene while PBP-C0 showed poor solubility in chloroform and chlorobenzene. The corresponding molecular weights were measured by using high-temperature gel-permeation chromatography. The number-average molecular weights (M_n) of the polymers PBP-C0, PBP-C8, and PBP-C6 were 12.2, 43.4 and 45.9 kDa with polymer dispersity index (PDI) of 1.60, 2.03 and 1.93, respectively. Thermogravimetric analysis (TGA) and differential scanning calorimetry (DSC) were used to investigate the thermal stability of all polymers as shown in Fig. S2 (in the electronic supplementary information, ESI). All the polymers have good

thermal stability, 5% weight loss was observed at 345, 435 and 428 ℃, of PBP-C0, PBP-C8 and PBP-C6, respectively. The corresponding DSC curves from 50 ℃ to 300 ℃ show no endothermic or exothermic peaks because the rigid conjugated backbones limit the motion of polymer chains.

RESULTS AND DISCUSSION

Optical and Electrochemical Properties

UV-Vis absorption spectra were tested in solution and film to determine the optical properties of polymers and the acceptor. Fig. 1(a) shows the normalized film UV-Vis absorption spectra of PBP-C0, PBP-C8, PBP-C6 and Y5. Absorption coefficients were measured in chlorobenzene as shown in Fig. 1(b). Both solution and film absorption spectra of polymers show two strong maximum absorption peaks below 500 nm and 500–700 nm. The absorption peak at a longer wavelength is associated with the intramolecular charge transfer (ICT) band. Whereas, the absorption peak at the shorter wavelength is associated with π-π^* transition along the conjugated backbone of polymers, a signature peak of dibenzo[*a*,*c*]phenazine based polymers.[51] The optical bandgaps of polymers were measured from film absorption onset, according to the equation of $E_g^{opt} = 1240/\lambda_{onset}$. The measured film absorption onsets were at 764, 716 and 745 nm for PBP-C0, PBP-C8, and PBP-C6, and their optical bandgap were 1.62, 1.73 and 1.67 eV, respectively. These optical property data are displayed in Table 1. The substituted bulky alkyl group on the thiophene π-bridge induces steric hindrance, which limits the effective conjugation along the conjugated backbone and consequently increases the optical bandgap. The red-shift over 25 nm in the ICT band can be observed for all polymers from solution to film, attributed to the formation of a more ordered microstructure in film. In addition, all the polymers display a complementary absorption profile with a Y5 acceptor, which is beneficial to harvest maximum solar energy.

The highest occupied molecular orbital (HOMO) and the lowest unoccupied molecular orbital (LUMO) energy levels of polymers and the acceptor were measured by cyclic voltammetry (CV). The CV curves of PBP-C0, PBP-C8, PBP-C6 and acceptor Y5 are shown in Fig. 1(c). E_{HOMO}/E_{LUMO} values are calculated as −3.54 eV/−5.48 eV, −3.58 eV/−5.57 eV and −3.54 eV/−5.50 eV, respectively. These values were used to plot the energy level diagrams as shown in Fig. 1(d). In general, the V_{OC} of devices depends upon the difference between E_{HOMO} (donors) and E_{LUMO} (acceptors) while excluding other influences, deeper the E_{HOMO} of donors more will be the V_{OC}. Therefore, a similar trend in V_{OC} is observed for PBP-C0, PBP-C6, PBP-C8 based devices when blended with Y5 acceptor as discussed in the next section.

Theoretical Calculations

To further investigate the effect of different substituted thiophene π-bridge on the molecular space geometry and electronic density distribution, theoretical calculations were performed by use of density functional theory (DFT) in the B3LYP/6-31G(d,p) level.[47] To reduce the computational cost, polymers were calculated as oligomers with two repeating units, and alkyl chains were replaced with methyl groups. As shown in Fig. S3

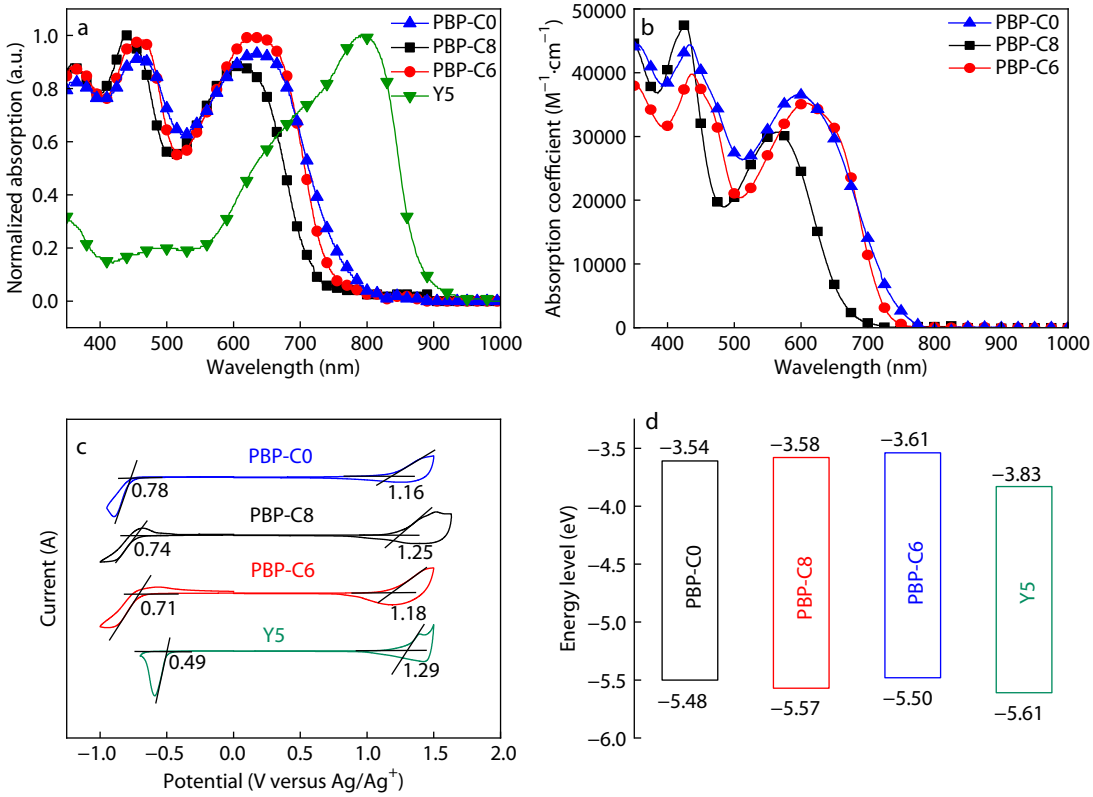

Fig. 1 (a) Normalized optical absorption spectra in film state, (b) absorption coefficient spectra in solution, (c) cyclic voltammograms and (d) energy level diagrams of the polymer donors PBP-C0, PBP-C8, PBP-C6 and acceptor Y5.

https://doi.org/10.1007/s10118-022-2719-z

Table 1 Physicochemical properties of PBP-C0, PBP-C8 and PBP-C6.

Materials	Solution		Film		E_g^{opt} (eV)	E_{HOMO} (eV)	E_{LUMO} (eV)	M_n (kDa)	PDI
	λ_{max} (nm)	α (M^{-1}·cm^{-1})	λ_{max} (nm)	λ_{onset} (nm)					
PBP-C0	433, 597	3.48×10^4	462, 631	764	1.62	−3.54	−5.48	12.2	1.60
PBP-C8	426, 564	4.75×10^4	441, 617	716	1.73	−3.58	−5.57	43.4	2.03
PBP-C6	436, 608	3.80×10^4	463, 632	745	1.67	−3.61	−5.50	45.9	1.93
Y5	719	18.4×10^4	795	876	1.42	−3.83	−5.61	–	–

(in ESI), the measured dihedral angles of PBP-C0, PBP-C8, and PBP-C6 between D-units and thiophene units are 9.3°, 29.2° and 25.0°, respectively. Similarly, the measured dihedral angles of PBP-C0, PBP-C8, and PBP-C6 between A-units and thiophene units are 15.7°, 11.9° and 11.9°, respectively. The lower dihedral angles are beneficial to make conjugated backbone planar and also to improve π-π stacking. Although PBP-C0 demonstrated the smallest dihedral angle among other polymers, poor solubility limited its device application. PBP-C8 has the bulky branched alkyl chain on π-bridge which induced the steric hindrance thus increasing the dihedral angle and attaining the twisted curvature geometry in calculated optimized structure. Furthermore, PBP-C6 possessed a moderate dihedral angle that resulted in an almost planar geometry with improved solubility, which is beneficial for efficient charge transportation.

Temperature-dependent Absorption

To study conformational behavior of polymers at different temperatures, temperature dependant UV-Vis absorptions spectra of PBP-C0, PBP-C8, and PBP-C6 were recorded in chlorobenzene with a gradual rise in the temperatures from 30 °C to 100 °C as shown in Fig. 2. Both PBP-C8 and PBP-C0 absorption spectra show a little blue-shift in the ICT absorption band with the rise in the temperature, suggesting a highly rigid conjugated backbone. Whereas, PBP-C6 shows a notable blue-shift in the ICT absorption band with the rise in the temperature, which suggests conformational freedom due to the flexible linear alkyl chain. Furthermore, the ICT absorption band of PBP-C8 has a lower intensity than the absorption band at the shorter wavelength, governs by the twisted curvature geometry. The twisted curvature geometry lowers the effective conjugation that resulted in the hypochromic shift of the ICT band. On the contrary, the ICT band of PBP-C6 shows relatively high absorption which indicates a planar conjugated backbone that ensures effective conjugation and greater charge mobility. These results are consistent with calculated optimized geometry by DFT calculations.

Photovoltaic Properties

To investigate the photovoltaic properties of each polymer, conventional devices were fabricated with device structure as shown in Fig. S1 (in ESI). The current density-voltage (*J*-*V*) plot of each device is shown in Fig. 3(a), and these data are displayed in Table 2. PBP-C8:Y5-based PSC has the higher V_{OC} of 0.938 V attributed to the lowest E_{HOMO} of PBP-C8 among the three polymers with low J_{SC} of 11.08 mA·cm^{-2}, an FF of 55.09%, which compromised PCE of 5.72%. The poor solubility of PBP-C0 limits the processability, which results in PBP-C0:Y5-based device unfavourable photovoltaic performance including a V_{OC} of 0.792 V, a J_{SC} of 10.33 mA·cm^{-2}, an FF of 37.13%, and a PCE of 3.04%. The devices based on PBP-C6:Y5 possesses a V_{OC} of 0.872 V, the best J_{SC} of 20.90 mA·cm^{-2} and the best FF of 61.26%, and the best PCE of 11.60% among the three devices.

External quantum efficiency (EQE) values of the three devices were measured at the wavelength range from 300 nm to 1000 nm as shown in Fig. 3(b). PBP-C6:Y5-based devices exhibits the maximum EQE values over 70%, which is beneficial

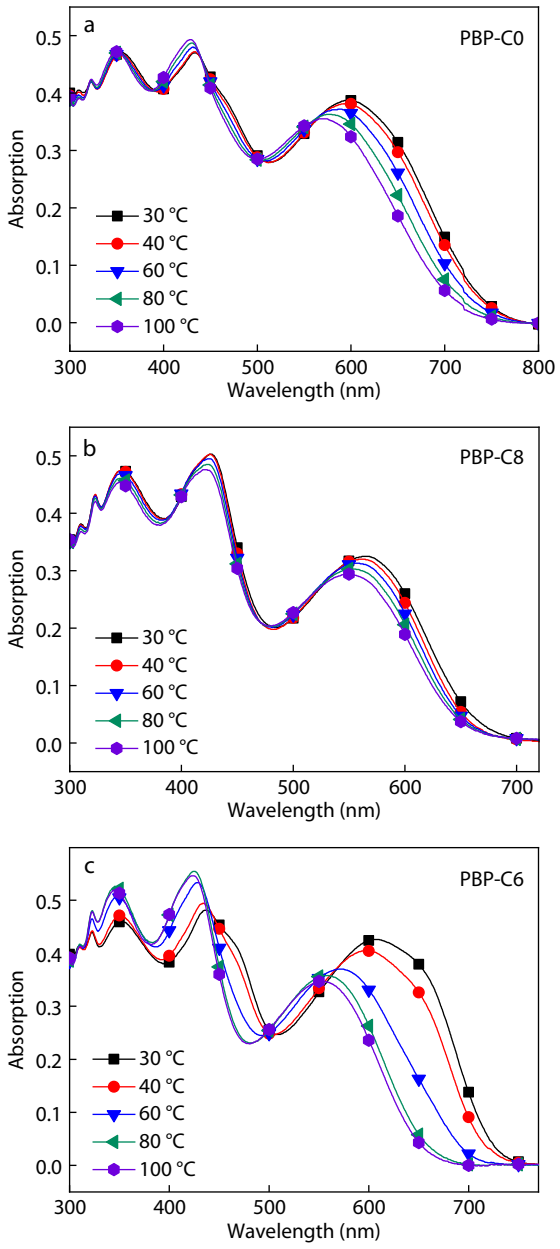

Fig. 2 Temperature-dependent absorption spectra of (a) PBP-C0, (b) PBP-C8 and (c) PBP-C6 in chlorobenzene.

https://doi.org/10.1007/s10118-022-2719-z

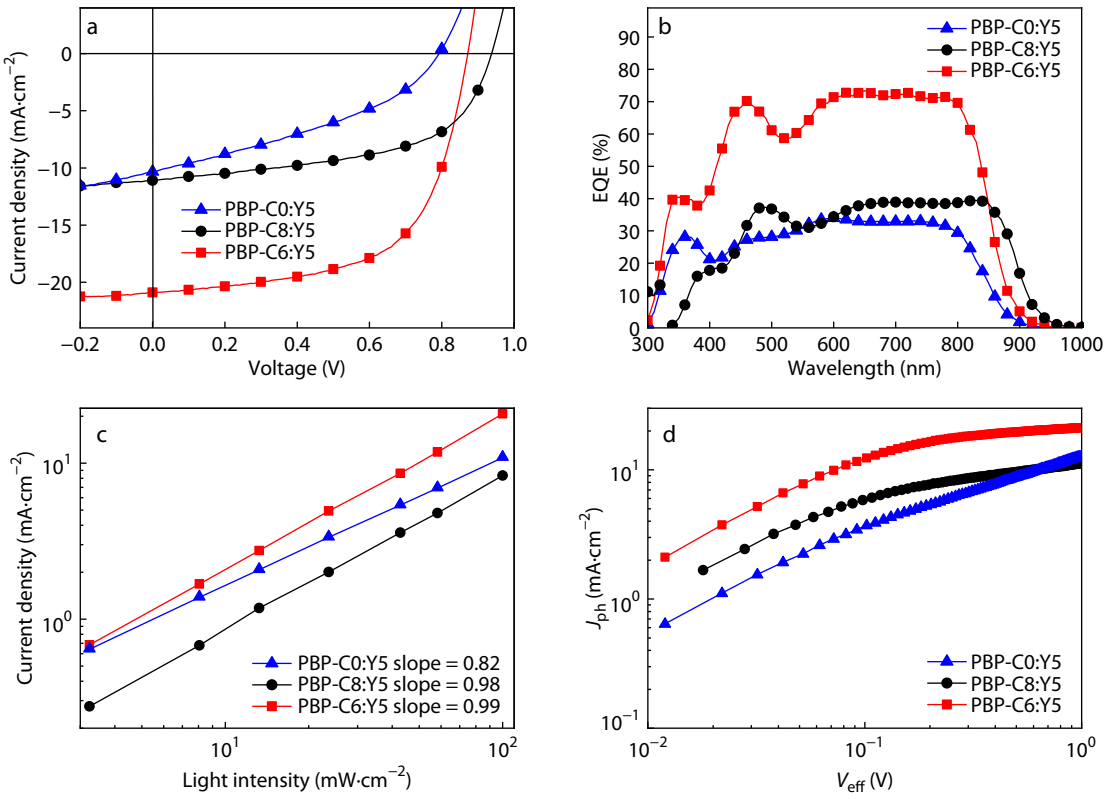

Fig. 3 The (a) *J-V* plots, (b) EQE plots, (c) J_{Ph} versus V_{eff}, and (d) J_{SC} versus the light intensity of PBP-C0, PBP-C8 and PBP-C6 based devices.

Table 2 Photovoltaic parameters for donors:Y5 devices.

	V_{OC} [a] (V)	J_{SC} [a] (mA·cm^{-2})	FF [a] (%)	PCE [a] (%)	$J_{SC,EQE}$ (mA·cm^{-2})
PBP-C0:Y5	0.792 (0.722±0.072)	10.33 (9.11±1.26)	37.13 (31.20±4.69)	3.04 (2.68±0.38)	10.29
PBP-C8:Y5	0.938 (0.920±0.027)	11.08 (9.95±1.11)	55.09 (52.23±5.62)	5.72 (5.01±0.67)	11.17
PBP-C6:Y5	0.872 (0.869±0.004)	20.90 (20.69±0.26)	61.26 (58.94±1.79)	11.60 (10.71±0.36)	20.64

[a] The average values of PCE were obtained from 10 independent cells.

to capture more light and obtain high J_{SC}. PBP-C8:Y5 and PBP-C0:Y5-based devices demonstrated weaker EQE values below 40% at the wavelength range from 300 nm to 1000 nm. The current density values are measured to be 10.29, 11.17 and 20.64 mA·cm^{-2} from PBP-C0:Y5, PBP-C8:Y5 and PBP-C6:Y5 based devices EQE curves, respectively, as shown in Table 2, respectively. The J_{SC} values calculated from EQE are the same as *J-V* curves, which proves the reliability of the photovoltaic parameters.

To study the charge recombination behavior in three different devices as shown in Fig. 3(c), the dependence of J_{SC} on different illumination intensities (P_{light}) was tested. To be specific, the relationship between J_{SC} and P_{light} follows the equation $J_{SC} \propto P_{light}$, the value (α) which is equal to the slope can reflect the degree of charge recombination. If α approach 1, it means that there is almost no bimolecular recombination happening in the active layer. The value (α) of 0.99 for the PBP-C6-based devices is more closed to 1 than the other two devices, which indicated efficient suppression of bimolecular recombination.

To gain more insight into the exciton dissociation, the relationship between photocurrent density (J_{Ph}) and effective voltage (V_{eff}) of the three devices were measured as shown in Fig. 3(d). Generally speaking, J_{Ph} is defined as the difference between the values of current density under 100 mW·cm^{-2} illumination and the value of current density in the dark. V_{eff} is defined as the equation of $V_{eff} = V_0 - V_a$, in which V_a is the applied voltage and V_0 is the voltage when J_{Ph} is 0. J_{Sat} is the saturated photocurrent density under a high V_{eff} over 2 V, where all photoinduced excitons dissociate into free carriers and are collected. P_{Diss} is defined as J_{Ph}/J_{Sat}, which can represent the degree of exciton dissociation. P_{Diss} values of PBP-C0, PBP-C8, and PBP-C6-based devices were measured as 25.9%, 56.9%, and 72.5%, respectively. PBP-C6-based device shows more effective exciton dissociation and charge collection, which give rise to a higher J_{SC}.

Hole and electron mobilities were measured by the space-charge-limited current (SCLC) method as shown in Fig. S4 and the results are listed in Table S1 (in ESI). The hole mobilities (μ_h) of PBP-C0, PBP-C8 and PBP-C6-based devices are 0.06×10^{-4}, 0.57×10^{-4} and 1.40×10^{-4} cm^2·V^{-1}·s^{-1}, respectively. Meanwhile, the electron mobility (μ_e) of the three devices are 0.48×10^{-4}, 1.48×10^{-4} and 2.12×10^{-4} cm^2·V^{-1}·s^{-1}, respectively. The satisfactory μ_h and μ_e of PBP-C6-based device led to high J_{SC} and PCE. In the meantime, PBP-C6-based device possesses the balanced hole/electron mobility (μ_h/μ_e) values as

https://doi.org/10.1007/s10118-022-2719-z

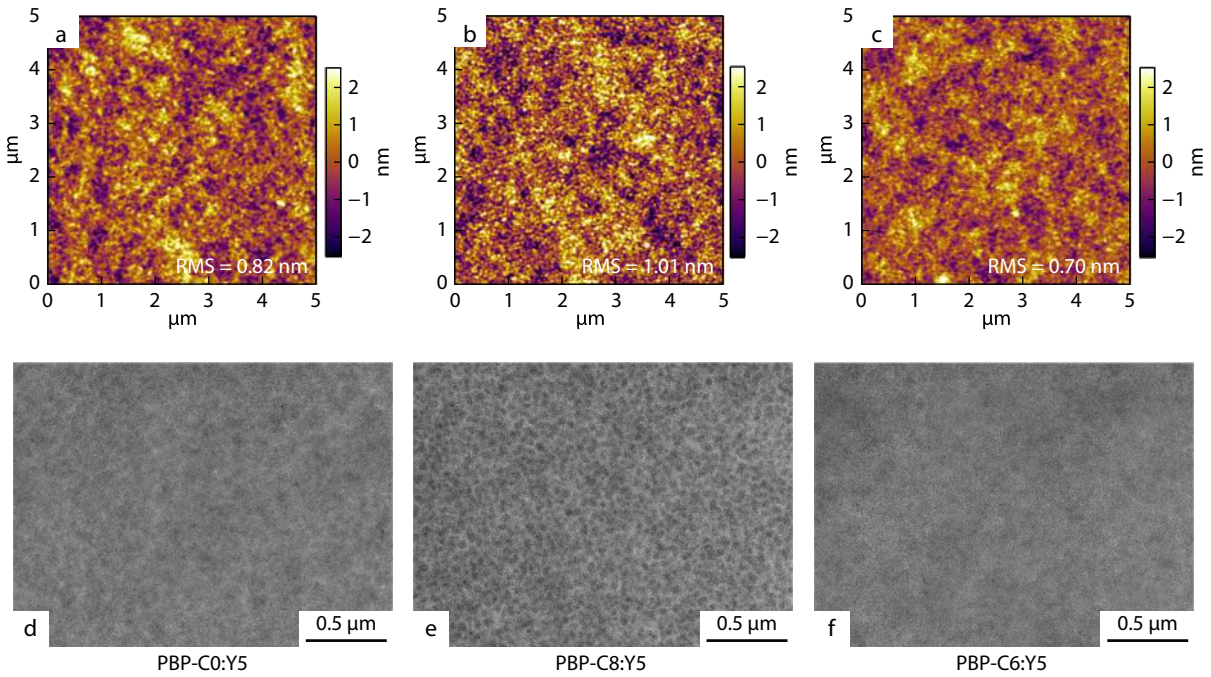

Fig. 4 (a–c) AFM (5 μm × 5 μm) and (d–f) TEM images of PBP-C0:Y5, PBP-C8:Y5 and PBP-C6:Y5 blend films.

0.66 when being compared with PBP-C0-based and PBP-C8 based devices as 0.13 and 0.39, respectively. A balanced μ_h/μ_e is beneficial to both charge transport and efficient carrier collection. Considering the highest hole and electron mobility, the most efficient exciton dissociation, and the less charge carrier recombination, PBP-C6-based device shows higher FF, J_{SC}, and PCE in three devices.

Morphology of Blend Film

The active layer with a smooth surface is essential for good photovoltaic performance, requires keeping a good contact between the adjacent hole and electron transporting layers. The root mean square (RMS) roughness of PBP-C0:Y5, PBP-C8:Y5, and PBP-C6:Y5 blend films were measured as 0.82, 1.01 and 0.70 nm, respectively, as shown in Figs. 4(a)–4(c). Among all the active layers, the PBP-C6:Y5 film exhibits the smallest RMS, which suggests both suitable compatibility and miscibility. Such morphological compatibility is beneficial to efficiently generate exciton, dissociate exciton, and transport charge carrier. The TEM results also show good consistency with the AFM data and TEM images are shown in Figs. 4(d)–4(f).

In contrast to PBP-C6:Y5 blend films, other blend films show slightly bigger domain sizes attributed to poor miscibility between donors and acceptors. The poor solubility of PBP-C0 limits the processability of PBP-C0:Y5 blend film that leads to overside self-aggregated domains. With the flexible linear alkyl group on π-bridge, PBP-C6:Y5-based devices show moderate domain sizes and phase separation, which contributed to more exciton generation, more efficient exciton dissociation, higher charge carrier transport, and finally led to a high PCE.

CONCLUSIONS

In summary, we synthesized and studied three dibenzo[*a*,*c*]phenazine based polymers, named PBP-C0, PBP-C8, and PBP-C6, with different substitutions: hydrogen atoms, 2-ethylhexyl, and *n*-hexyl groups on the π-bridge, respectively. The steric hindrance induced by the bulky alkyl group on the π-bridge twisted the conjugated backbone thereby increasing the optical bandgap and exhibiting poor blend film morphology. Both PBP-C0:Y5 and PBP-C8:Y5 blend films showed bigger domain sizes caused by the poor solubility and rigid twisted geometry, respectively. This lowered the exciton generation and dissociation, charge carrier mobility, and photovoltaic performance. On the contrary, the *n*-hexyl substituted polymer PBP-C6 based devices exhibited much better charge mobility, exciton dissociation, and optimum domain attributed to the planar curvature geometry and good solubility. We have achieved the PCE of PBP-C6 based devices as 11.60% with a V_{OC} of 0.872 V, a J_{SC} of 20.90 mA·cm^{-1}, and an FF of 61.26%. These results highlight the positive effects of the moderate size alkyl chains on the π-bridges as an effective strategy to tune the solubility, energy levels, absorption, morphology of the donor polymers to enhance the photovoltaic performance.

NOTES

The authors declare no competing financial interest.

Electronic Supplementary Information

Electronic supplementary information (ESI) is available free of charge in the online version of this article at http://doi.org/10.1007/s10118-022-2719-z.

ACKNOWLEDGMENTS

This work was financially supported by the National Natural

Science Foundation of China (Nos. 21733005 and 21975115), the Shenzhen Fundamental Research Program (Nos. JCYJ20190809163011543, JCYJ20200109140801751 and JCYJ20210324120010028), the Guangdong Provincial Key Laboratory of Catalysis (No. 2020B121201002), the Guangdong Innovative and Entrepreneurial Research Team Program (No. 2016ZT06G587), and the Shenzhen Sci-Tech Fund (No. KYTDPT 20181011104007). We also thank the SUSTech Core Research Facilities for AFM and TEM measurements.

REFERENCES

1 Li, Y.; Xu, G.; Cui, C.; Li, Y. Flexible and semitransparent organic solar cells. *Adv. Energy. Mater.* **2018**, *8*, 1701791.
2 Xu, Y.; Yao, H.; Hou, J. Recent advances in fullerene-free polymer solar cells: materials and devices. *Chin. J. Chem.* **2019**, *37*, 207–215.
3 Chen, J.; Cao, Y. Development of novel conjugated donor polymers for high-efficiency bulk-heterojunction photovoltaic devices. *Acc. Chem. Res.* **2009**, *42*, 1709–1718.
4 Li, Y. Molecular design of photovoltaic materials for polymer solar cells: toward suitable electronic energy levels and broad absorption. *Acc. Chem. Res.* **2012**, *45*, 723–733.
5 Cheng, Y. J.; Yang, S. H.; Hsu, C. S. Synthesis of conjugated polymers for organic solar cell applications. *Chem. Rev.* **2009**, *109*, 5868–5923.
6 Cui, C.; Li, Y. High-performance conjugated polymer donor materials for polymer solar cells with narrow-bandgap nonfullerene acceptors. *Energy Environ. Sci.* **2019**, *12*, 3225–3246.
7 Li, G.; Zhu, R.; Yang, Y. Polymer solar cells. *Nat. Photonics* **2012**, *6*, 153–161.
8 Duan, C.; Ding, L. The new era for organic solar cells: polymer donors. *Sci. Bull.* **2020**, *65*, 1422–1424.
9 Duan, C.; Ding, L. The new era for organic solar cells: polymer acceptors. *Sci. Bull.* **2020**, *65*, 1508–1510.
10 Bi, P.; Zhang, S.; Wang, J.; Ren, J.; Hou, J. Progress in organic solar cells: materials, physics and device engineering. *Chin. J. Chem.* **2021**, *39*, 2607–2625.
11 Yuan, J.; Zhang, Y.; Zhou, L.; Zhang, G.; Yip, H. L.; Lau, T. K.; Lu, X.; Zhu, C.; Peng, H.; Johnson, P. A.; Leclerc, M.; Cao, Y.; Ulanski, J.; Li, Y.; Zou, Y. Single-junction organic solar cell with over 15% efficiency using fused-ring acceptor with electron-deficient core. *Joule* **2019**, *3*, 1140–1151.
12 Zhang, M.; Guo, X.; Ma, W.; Ade, H.; Hou, J. A large-bandgap conjugated polymer for versatile photovoltaic applications with high performance. *Adv. Mater.* **2015**, *27*, 4655–4660.
13 Zhang, Z.; Li, Y.; Cai, G.; Zhang, Y.; Lu, X.; Lin, Y. Selenium heterocyclic electron acceptor with small urbach energy for as-cast high-performance organic solar cells. *J. Am. Chem. Soc.* **2020**, *142*, 18741–18745.
14 Zhang, Y.; Cai, G.; Li, Y.; Zhang, Z.; Li, T.; Zuo, X.; Lu, X.; Lin, Y. An electron acceptor analogue for lowering trap density in organic solar cells. *Adv. Mater.* **2021**, *33*, 2008134.
15 Jiang, K.; Wei, Q.; Lai, J. Y. L.; Peng, Z.; Kim, H. K.; Yuan, J.; Ye, L.; Ade, H.; Zou, Y.; Yan, H. Alkyl chain tuning of small molecule acceptors for efficient organic solar cells. *Joule* **2019**, *3*, 3020–3033.
16 Gao, K.; Kan, Y.; Chen, X.; Liu, F.; Kan, B.; Nian, L.; Wan, X.; Chen, Y.; Peng, X.; Russell, T. P.; Cao, Y.; Jen, A. K. Y. Low-bandgap porphyrins for highly efficient organic solar cells: materials, morphology, and applications. *Adv. Mater.* **2020**, *32*, 1906129.
17 Zhang, M.; Zhu, L.; Zhou, G.; Hao, T.; Qiu, C.; Zhao, Z.; Hu, Q.; Larson, B. W.; Zhu, H.; Ma, Z.; Tang, Z.; Feng, W.; Zhang, Y.; Russell, T. P.; Liu, F. Single-layered organic photovoltaics with double cascading charge transport pathways: 18% efficiencies. *Nat. Commun.* **2021**, *12*, 309.
18 Ma, Q.; Jia, Z.; Meng, L.; Zhang, J.; Zhang, H.; Huang, W.; Yuan, J.; Gao, F.; Wan, Y.; Zhang, Z.; Li, Y. Promoting charge separation resulting in ternary organic solar cells efficiency over 17. 5%. *Nano Energy* **2020**, *78*, 105272.
19 Ma, R.; Liu, T.; Luo, Z.; Guo, Q.; Xiao, Y.; Chen, Y.; Li, X.; Luo, S.; Lu, X.; Zhang, M.; Li, Y.; Yan, H. Improving open-circuit voltage by a chlorinated polymer donor endows binary organic solar cells efficiencies over 17%. *Sci. China Chem.* **2020**, *63*, 325–330.
20 Firdaus, Y.; Le Corre, V. M.; Karuthedath, S.; Liu, W.; Markina, A.; Huang, W.; Chattopadhyay, S.; Nahid, M. M.; Nugraha, M. I.; Lin, Y.; Seitkhan, A.; Basu, A.; Zhang, W.; McCulloch, I.; Ade, H.; Labram, J.; Laquai, F.; Andrienko, D.; Koster, L. J. A.; Anthopoulos, T. D. Long-range exciton diffusion in molecular non-fullerene acceptors. *Nat. Commun.* **2020**, *11*, 5220.
21 Hou, R.; Li, M.; Ma, X.; Huang, H.; Lu, H.; Jia, Q.; Liu, Y.; Xu, X.; Li, H. B.; Bo, Z. Noncovalently fused-ring electron acceptors with C_{2v} symmetry for regulating the morphology of organic solar cells. *ACS Appl. Mater. Interfaces* **2020**, *12*, 46220–46230.
22 Nian, L.; Kan, Y.; Gao, K.; Zhang, M.; Li, N.; Zhou, G.; Jo, S. B.; Shi, X.; Lin, F.; Rong, Q.; Liu, F.; Zhou, G.; Jen, A. K. Y. Approaching 16% efficiency in all-small-molecule organic solar cells based on ternary strategy with a highly crystalline acceptor. *Joule* **2020**, *4*, 2223–2236.
23 Liu, Q.; Fang, J.; Wu, J.; Zhu, L.; Guo, X.; Liu, F.; Zhang, M. Tuning aggregation behavior of polymer donor *via* molecular-weight control for achieving 17.1% efficiency inverted polymer solar cells. *Chin. J. Chem.* **2021**, *39*, 1941–1947.
24 Chao, P.; Chen, H.; Zhu, Y.; Lai, H.; Mo, D.; Zheng, N.; Chang, X.; Meng, H.; He, F. A benzo[1,2-*b*:4,5-*c*']dithiophene-4,8-dione-based polymer donor achieving an efficiency over 16. *Adv. Mater.* **2020**, *32*, 1907059.
25 Liu, Q.; Jiang, Y.; Jin, K.; Qin, J.; Xu, J.; Li, W.; Xiong, J.; Liu, J.; Xiao, Z.; Sun, K.; Yang, S.; Zhang, X.; Ding, L. 18% Efficiency organic solar cells. *Sci. Bull.* **2020**, *65*, 272–275.
26 Zhao, T.; Wang, H.; Pu, M.; Lai, H.; Chen, H.; Zhu, Y.; Zheng, N.; He, F. Tuning the molecular weight of chlorine-substituted polymer donors for small energy loss. *Chin. J. Chem.* **2021**, *39*, 1651–1658.
27 Zhang, G.; Ning, H.; Chen, H.; Jiang, Q.; Jiang, J.; Han, P.; Dang, L.; Xu, M.; Shao, M.; He, F.; Wu, Q. Naphthalenothiophene imide-based polymer exhibiting over 17% efficiency. *Joule* **2021**, *5*, 931–944.
28 Zhu, C.; Meng, L.; Zhang, J.; Qin, S.; Lai, W.; Qiu, B.; Yuan, J.; Wan, Y.; Huang, W.; Li, Y. A quinoxaline-based D-A copolymer donor achieving 17. 62% efficiency of organic solar cells. *Adv. Mater.* **2021**, *33*, 2100474.
29 Sun, C.; Pan, F.; Bin, H.; Zhang, J.; Xue, L.; Qiu, B.; Wei, Z.; Zhang, Z. G.; Li, Y. A low cost and high performance polymer donor material for polymer solar cells. *Nat. Commun.* **2018**, *9*, 743.
30 Song, H. J.; Lee, T. H.; Han, M. H.; Lee, J. Y.; Moon, D. K. Synthesis of donor-acceptor polymers through control of the chemical structure: improvement of PCE by planar structure of polymer backbones. *Polymer* **2013**, *54*, 1072–1079.
31 Song, H. J.; Lee, E. J.; Kim, D. H.; Lee, S. M.; Lee, J. Y.; Moon, D. K. Enhancement of external quantum efficiency through steric hindrance of phenazine derivative for white polymer light-emitting diode materials. *Synth. Met.* **2013**, *181*, 98–103.
32 Zhang, Y.; Zou, J.; Yip, H. L.; Chen, K. S.; Zeigler, D. F.; Sun, Y.; Jen, A. K. Y. Indacenodithiophene and quinoxaline-based conjugated polymers for highly efficient polymer solar cells. *Chem. Mater.* **2011**, *23*, 2289–2291.
33 He, R.; Yu, L.; Cai, P.; Peng, F.; Xu, J.; Ying, L.; Chen, J.; Yang, W.; Cao, Y. Narrow-band-gap conjugated polymers based on 2,7-dioctyl substituted dibenzo[*a*,*c*]phenazine derivatives for

polymer solar cells. *Macromolecules* **2014**, *47*, 2921−2928.
34 Lee, T. H.; Choi, M. H.; Jeon, S. J.; Nam, S. J.; Han, Y. W.; Haw, J. R.; Moon, D. K. Improvement of short circuit current density by intermolecular interaction between polymer backbones for polymer solar cells. *Polym. J.* **2017**, *49*, 177−187.
35 Sun, Y.; Zhang, C.; Dai, B.; Lin, B.; Yang, H.; Zhang, X.; Guo, L.; Liu, Y. Side chain engineering and conjugation enhancement of benzodithiophene and phenanthrenequnioxaline based conjugated polymers for photovoltaic devices. *J. Polym. Sci., Part A: Polym. Chem.* **2015**, *53*, 1915−1926.
36 Jo, E.; Park, J. B.; Lee, W. H.; Kim, J. H.; Jung, I. H.; Hwang, D. H.; Kang, I. N. Synthesis and characterization of a new phenanthrenequinoxaline-based polymer for organic solar cells. *J. Polym. Sci., Part A: Polym. Chem.* **2016**, *54*, 2804−2810.
37 Hu, T.; Han, L.; Xiao, M.; Bao, X.; Wang, T.; Sun, M.; Yang, R. Enhancement of photovoltaic performance by increasing conjugation of the acceptor unit in benzodithiophene and quinoxaline copolymers. *J. Mater. Chem. C* **2014**, *2*, 8047−8053.
38 Mei, J.; Bao, Z. Side chain engineering in solution-processable conjugated polymers. *Chem. Mater.* **2014**, *26*, 604−615.
39 Osaka, I.; Saito, M.; Koganezawa, T.; Takimiya, K. Thiophene-thiazolothiazole copolymers: significant impact of side chain composition on backbone orientation and solar cell performances. *Adv. Mater.* **2014**, *26*, 331−338.
40 Zhang, C.; Sun Y.; Dai B.; Zhang, X. Q.; Yang, H.; Lin, B. P.; Guo, L. X. Resent progress in side-chain engineering of organic photovoltaic conjugated polymer. *Chin. J. Org. Chem.* **2014**, *34*, 1701−1716.
41 Li, G.; Zhao, B.; Kang, C.; Lu, Z.; Li, C.; Dong, H.; Hu, W.; Wu, H.; Bo, Z. Side chain influence on the morphology and photovoltaic performance of 5-fluoro-6-alkyloxybenzothiadiazole and benzodithiophene based conjugated polymers. *ACS Appl. Mater. Interfaces* **2015**, *7*, 10710−10717.
42 Osaka, I.; Takimiya, K. Backbone orientation in semiconducting polymers. *Polymer* **2015**, *59*, A1−A15.
43 Jin, Y.; Chen, Z.; Dong, S.; Zheng, N.; Ying, L.; Jiang, X. F.; Liu, F.; Huang, F.; Cao, Y. A novel naphtho[1,2-*c*:5,6-*c*']bis([1,2,5]thiadiazole)-based narrow-bandgap *π*-conjugated polymer with power conversion efficiency over 10%. *Adv. Mater.* **2016**, *28*, 9811−9818.
44 Kim, J. H.; Wood, S.; Park, J. B.; Wade, J.; Song, M.; Yoon, S. C.; Jung, I. H.; Kim, J. S.; Hwang, D. H. Optimization and analysis of conjugated polymer side chains for high-performance organic photovoltaic cells. *Adv. Funct. Mater.* **2016**, *26*, 1517−1525.
45 Dutta, P.; Park, H.; Lee, W. H.; Kang, I. N.; Lee, S. H. Synthesis characterization and bulk-heterojunction photovoltaic applications of new naphtho[1,2-*b*:5,6-*b*']dithiophene–quinoxaline containing narrow band gap D-A conjugated polymers. *Polym. Chem.* **2014**, *5*, 132−143.
46 El-Shehawy, A. A.; Abdo, N. I.; El-Hendawy, M. M.; Abdallah, A. R. I. A.; Lee, J. S. Dialkylthienosilole and *N*-alkyldithienopyrrole-based copolymers: synthesis, characterization, and photophysical study. *J. Phys. Org. Chem.* **2020**, *33*, e4063.
47 Du, M.; Geng, Y.; Ji, H.; Li, G.; Xiao, Y.; Zuo, K.; Liu, Y.; Guo, Q.; Tang, A.; Zhou, E. The optimization of *π*-bridge for trialkylsilyl substituted D-*π*-A photovoltaic polymers. *Dyes Pigm.* **2021**, *194*, 109609.
48 Rehman, T.; Liu, Z. X.; Lau, T. K.; Yu, Z. P.; Shi, M.; Lu, X.; Li, C. Z.; Chen, H. Influence of bridging groups on the photovoltaic properties of wide bandgap poly(BDTT-*alt*-BDD)s. *ACS Appl. Mater. Interfaces* **2019**, *11*, 1394−1401.
49 Mondal, R.; Ko, S.; Verploegen, E.; Becerril, H. A.; Toney, M. F.;Bao, Z. Side chain engineering of fused aromatic thienopyrazine based low band-gap polymers for enhanced charge carrier mobility. *J. Mater. Chem.* **2011**, *21*, 1537−1543.
50 Lee, Y.; Nam, Y. M.; Jo, W. H. Enhanced device performance of polymer solar cells by planarization of quinoxaline derivative in a low-bandgap polymer. *J. Mater. Chem.* **2011**, *21*, 8583−8590.
51 Körzdörfer, T.; Brédas, J. L. Organic electronic materials: recent advances in the DFT description of the ground and excited states using tuned range-separated hybrid functionals. *Acc. Chem. Res.* **2014**, *47*, 3284−3291.

https://doi.org/10.1007/s10118-022-2719-z